

## On the GeV emission of the type I BdHN GRB 130427A

R. RUFFINI,<sup>1,2,3,4,5</sup> R. MORADI,<sup>1,2</sup> J. A. RUEDA,<sup>1,2,4,6</sup> L. BECERRA,<sup>7</sup> C. L. BIANCO,<sup>1,2,6</sup> C. CHERUBINI,<sup>2,8</sup> S. FILIPPI,<sup>2,8</sup>  
Y. C. CHEN,<sup>1,2</sup> M. KARLICA,<sup>1,2,3</sup> N. SAHAKYAN,<sup>2,9</sup> Y. WANG,<sup>1,2</sup> AND S. S. XUE<sup>1,2</sup>

<sup>1</sup>ICRA, Dipartimento di Fisica, Sapienza Università di Roma, P.le Aldo Moro 5, 00185 Rome, Italy

<sup>2</sup>ICRANet, P.zza della Repubblica 10, 65122 Pescara, Italy

<sup>3</sup>Université de Nice Sophia Antipolis, CEDEX 2, Grand Château Parc Valrose, Nice, France

<sup>4</sup>ICRANet-Rio, Centro Brasileiro de Pesquisas Físicas, Rua Dr. Xavier Sigaud 150, 22290-180 Rio de Janeiro, Brazil

<sup>5</sup>INAF, Viale del Parco Mellini 84, 00136 Rome, Italy.

<sup>6</sup>INAF, Istituto di Astrofisica e Planetologia Spaziali, Via Fosso del Cavaliere 100, 00133 Rome, Italy.

<sup>7</sup>Escuela de Física, Universidad Industrial de Santander, A.A.678, Bucaramanga, 680002, Colombia

<sup>8</sup>ICRA and Department of Engineering, University Campus Bio-Medico of Rome, Via Alvaro del Portillo 21, 00128 Rome, Italy

<sup>9</sup>ICRANet-Armenia, Marshall Baghramian Avenue 24a, Yerevan 0019, Armenia

### ABSTRACT

It has been shown recently that the *inner engine* of a type I binary-driven hypernova (BdHN) is composed of a uniform background magnetic field of  $10^{14}$  G aligned with the rotation axis of a Kerr black hole modeled by the Wald solution. It is shown here using GRB 130427A as a prototype that this inner engine acts in a sequence of *elementary impulses*. The case of a single impulse was previously examined, showing that it can accelerate protons to  $\sim 10^{21}$  eV which, when propagating along the polar axis,  $\theta = 0$ , gives rise to ultra-high energy cosmic rays. We show here that when propagating with  $\theta \neq 0$ , the *inner engine* gives rise by synchrotron emission to GeV, TeV and PeV radiation. In this article we examine the sequence of such elementary impulses and determine their characteristic repetition times which start at  $\sim 10^{-6}$  s, slowly increase with time evolution. In principle, this “*inner engine*” can operate in a GRB for thousands of years. By scaling the BH mass and the magnetic field the same “*inner engine*” can describe as well active galactic nuclei (AGN).

**Keywords:** gamma-ray bursts: general — binaries: general — stars: neutron — supernovae: general — black hole physics

### 1. INTRODUCTION

Nine subclasses of gamma-ray bursts (GRBs) with binary progenitors have been recently introduced in Ruffini et al. (2016b, 2018b); Rueda et al. (2018); Wang et al. (2019). One of the best prototypes of the long GRBs emitting 0.1–100 GeV radiation is GRB 130427A (Ruffini et al. 2015). It belongs to a special subclass of GRBs originating from a tight binary system, of orbital period  $\sim 5$  min, composed of a carbon-oxygen core (CO<sub>core</sub>) undergoing a supernova (SN) event, in presence of a neutron star (NS) companion. The SN, as usual, gives rise to a new NS ( $\nu$ NS). For binary periods  $\lesssim 5$  min the hypercritical accretion of the SN ejecta onto the companion NS leads it to exceed the critical mass for gravitational collapse and form a Kerr black hole (BH). We have called these systems binary-driven hypernovae of type I (BdHNe I) with  $E_{\text{iso}} > 10^{52}$  erg as opposed to BdHNe II with  $E_{\text{iso}} < 10^{52}$  erg when the NS critical mass is not exceeded (Wang et al. 2019). Figure 1 shows

the ejecta density distribution of a BdHN I on the binary equatorial plane (left panel) and in a plane orthogonal to it (right panel), at the moment of gravitational collapse of the NS companion, namely at the moment of BH formation. These plots are the result of three-dimensional, numerical smoothed-particle-hydrodynamic (SPH) simulations of BdHNe recently described in Becerra et al. (2019).

In the specific case of GRB 130427A this BdHN I is seen from “the top” with the viewing angle in a plane orthogonal to the plane of the orbit of the binary progenitor. This allows us to follow all the details of the high energy activities around the BH. This includes: a) the observation of shock breakout b) the observation of the ultrarelativistic prompt emission (UPE) following the BH formation (Ruffini et al. 2018d), c) the feedback of the SN ejecta accreting on the  $\nu$ NS leading to the X-ray afterglow (Ruffini et al. 2018a), d) the ultra-high energy process extracting the rotational energy of the BH and

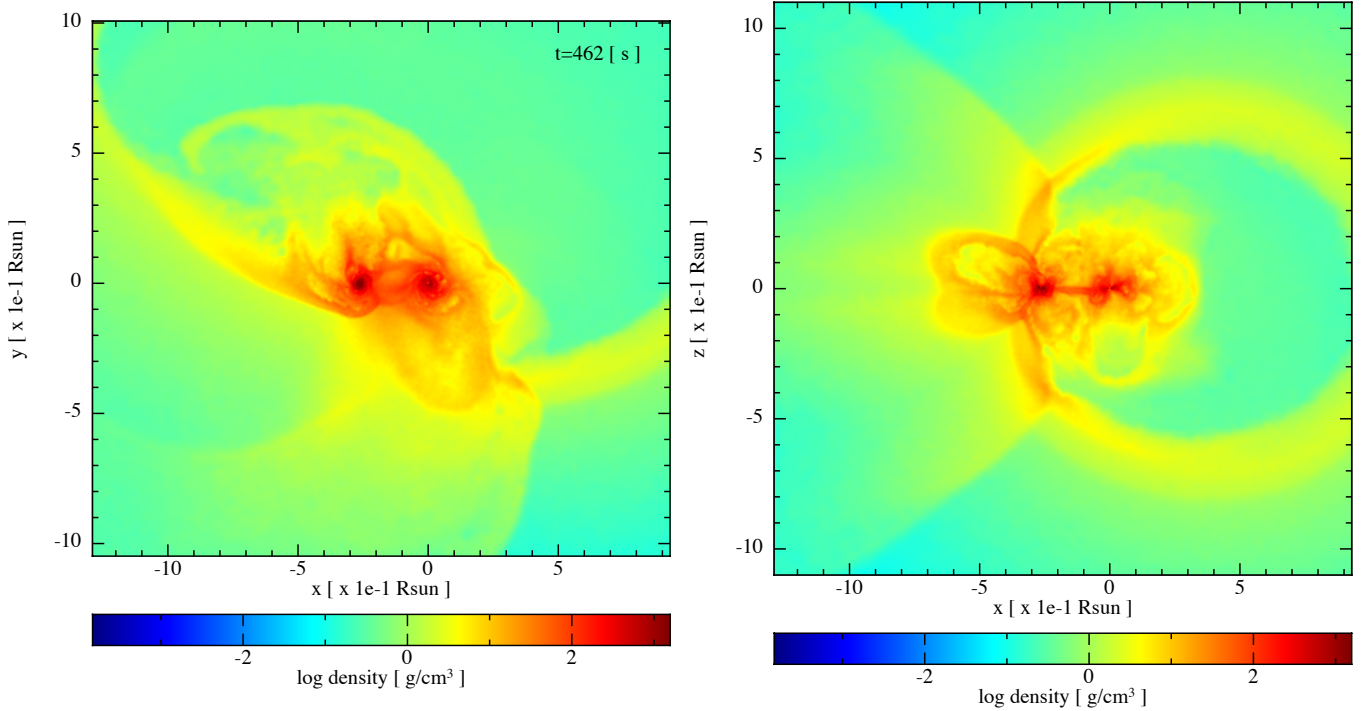


**Figure 1.** Selected SPH simulation from Becerra et al. (2019) of the exploding CO<sub>core</sub> as SN in the presence of a companion NS: Model ‘25m1p07e’ with  $P_{\text{orb}} \approx 5$  min. The CO<sub>core</sub> is taken from the 25  $M_{\odot}$  zero-age main-sequence (ZAMS) progenitor, so it has a mass  $M_{\text{CO}} = 6.85 M_{\odot}$ . The mass of the NS companion is  $M_{\text{NS}} = 2 M_{\odot}$ . The plots show the surface density on the equatorial binary plane (left panel) and on a plane orthogonal to it (right panel) at the time in which the NS companion reaches the critical mass and collapses to a BH,  $t = 462$  s from the SN shock breakout ( $t = 0$  of our simulation). The coordinate system has been rotated and translated in such a way that the NS companion is at the origin and the  $\nu$ NS is along the  $-x$  axis.

generating the GeV, TeV and PeV radiation treated in this article. The acceleration process of the protons and their emission of synchrotron radiation is also outlined in this article in Section 4 and Section 5.

Soon after the BH formation, approximately  $10^{57}$  baryons, which include the ones composing the NS companion, are enclosed in the BH horizon beyond any possible measurable effect apart from the total mass and spin of the BH.

A cavity of approximately  $10^{11}$  cm is formed around the BH with a finite density of  $10^{-6}$  g cm $^{-3}$ , see (Becerra et al. 2018, 2019). The evolution of such a cavity following the GRB explosion and its overtones inside the cavity has been addressed in the joint article, finally reaching a density of  $10^{-13}$  g cm $^{-3}$  inside the cavity.

The Kerr BH formation occurs in such a cavity in presence of an external, uniform magnetic field of  $B_0 \sim 10^{14}$  G aligned with the BH rotation axis. This *composite system* is the “inner engine” of the GRB and is mathematically described by the Wald solution (Wald 1974; Ruffini et al. 2018e; Rueda et al. 2019).

It is appropriate to recall that fields on the order of  $10^{14}$  G are routinely adopted in the description of the

afterglow both in the case of BdHNe I (Ruffini et al. 2018a), where dipole + quadrupole magnetic fields are adopted and as well for the case of BdHNe II (Wang et al. 2019).

We have here assumed that the magnetic field and the BH spin are antiparallel so protons along and near the rotation axis in the surrounding ionized circumburst medium are repelled from and electrons pulled in towards the BH. The assumption of a uniform field is expected to be valid only at distances close to the BH horizon. As pointed out by Gibbons et al. (2013), the stability of Wald-like solutions is guaranteed only if the uniform field is confined to a radius smaller than the Melvin radius,

$$R_M \sim 2/B_0, \quad (1)$$

which imposes an upper limit for this geometry of about  $10^{11}$  cm in our present case<sup>1</sup>. We are going to show in this article that the particle acceleration occurs near the

<sup>1</sup> The conversion factor from CGS to geometric units for the magnetic field is:  $\sqrt{G}/c^2 \approx 2.86 \times 10^{-25}$ , where  $G$  and  $c$  are the gravitational constant and speed of light in CGS units, respectively. Therefore a magnetic field on the order of  $10^{14}$  G in

BH horizon at distance of approximately  $10^5$  cm, much smaller than  $R_M$ .

Our main goal in this article is to develop a consistent “inner engine” model of the GeV and high-energy emissions from GRB 130427A. The model makes use of: 1) the rotational energy of the BH as its energy source; 2) the acceleration process of protons near the horizon of the BH implied by the electrodynamical properties of the Wald solution and 3) the emission of GeV-TeV-PeV by the synchrotron radiation in the magnetosphere of the Wald solution which is shown as well to imply the emission of the ultra-high energy cosmic rays (UHE-CRs) in the direction of the polar axis. As a byproduct of this approach we prove that the high-energy emission of GRB 130427A, contrary to the traditional approach based on continuous process, actually occurs in a repetitive sequence of discrete quantized “*elementary impulsive events*”. Each elementary event radiates an energy of the order of  $10^{44}$  erg, emitted every  $\sim 10^{-6}$  s, each leading to a depletion of  $10^{-9}$  times of the rotational energy of the Kerr BH. All the above leads to the conclusion that the high-energy emission process can indeed last for thousands of years.

A selected energy extraction history from a Kerr BH is addressed in section 2. The identification of the energy source in the rotational energy of a Kerr BH and correspondingly the mass and spin of the BH are determined in section 3. The electrodynamics of the “inner engine” is presented in section 4. The synchrotron radiation which is not emitted continuously but in discrete elementary processes lasting  $10^{-6}$  s is also presented in section 5. The sequence of the impulsive events and their repetition time are indicated in section 6. In section 7 preliminary inferences from the observation of GRB 190114C are addressed. In the conclusion we also outline the mounting evidence that this system, here developed for the Wald solution applied for GRB 130427A, is indeed the basis for the analysis of GRB 190114C (Ruffini et al. 2019b) and that it may well be extended to the much more massive BHs of  $10^9 M_\odot$  in AGN such as M87.

Before proceeding further let us recall that we impose as the starting point of our analysis the value of  $T_{50}$ , namely  $t_{\text{rf}}=37$  s of GBM data, with  $t_{\text{rf}}$  being the rest-frame time and  $T_{50}$  as the time during which the cumulative count increase from 5% to 55% above the background, thus encompassing 50% of total GRB counts; see Fig. 2.

geometric units is  $\approx 2 \times 10^{-25} \times 10^{14} \approx 2 \times 10^{-11} \text{ cm}^{-1}$  which leads to the Melvin radius of  $R = 2/B_0 \approx 10^{11} \text{ cm}$ .

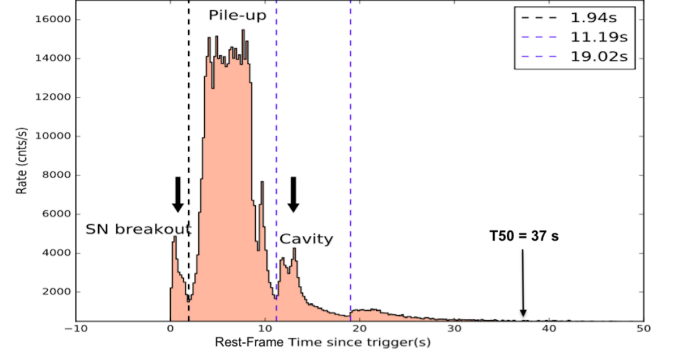


**Figure 2.** Count rate of GRB 130427A with isotropic energy  $E_{\text{iso}} = 1.4 \times 10^{54}$  erg and  $z = 0.34$ . The event count rate of n9 and n10 of Fermi-GBM surpasses  $\sim 8 \times 10^4$  counts per second in the prompt radiation between  $T_0 + 4.5$  s and  $T_0 + 11.5$  s. The GRB is there affected by pile-up, which significantly deforms the spectrum (Ackermann et al. 2014). We therefore impose as the starting point of our analysis the value of  $T_{50}$ , namely  $t_{\text{rf}}=37$  s, with  $t_{\text{rf}}$  being the rest-frame time, and cover all the successive Fermi-LAT data; see Fig. 3a. The above light curve has been derived from Fermi-GBM data (Ackermann et al. 2014) and the corresponding time-resolved spectral analysis independently is performed by Liang Li et al., 2019 (to be published).

## 2. ON SELECTED ENERGY EXTRACTION PROCESS FROM THE KERR BH

The determination of the mass-energy formula for a Kerr-Newman solution was reached in a rapid time sequence from September 17, 1970 by Christodoulou (1970) to March 1, 1971, by Christodoulou & Ruffini (1971), followed soon after on March 11, 1971, by the equivalent paper by Hawking (1971). The mass-formula, as formulated in Christodoulou & Ruffini (1971), reads

$$M^2 = \frac{J^2}{4M_{\text{irr}}^2} + \left( \frac{Q^2}{4M_{\text{irr}}^2} + M_{\text{irr}} \right)^2, \quad (2.1)$$

$$S = 16\pi M_{\text{irr}}^2 \quad (2.2)$$

$$\delta S = 32\pi M_{\text{irr}} \delta M_{\text{irr}} \geq 0, \quad (2.3)$$

where  $Q$ ,  $J$  and  $M$  are the three independent parameters of the Kerr-Newman geometry: the charge, the angular momentum and the mass in  $c = G = 1$  units.  $M_{\text{irr}}$  and  $S$  are respectively the derived quantities representing the irreducible mass and the horizon surface area.

In parallel, using these formulae, the concept of the BH was introduced by Ruffini & Wheeler (1971) as a physical and astrophysical entity to be tested and confronted with observation.

The first example of using the rotational energy of a BH for accelerating particles up to the high energy of  $10^{21}$  eV, using the charge and angular momentum of a

Kerr-Newman BH, was presented in Damour & Ruffini (1975), who also considered the vacuum polarization process leading to an  $e^+e^-$  optically thick plasma near the BH horizon. The Lorentz invariant formulation of the Kerr-Newman solution, implying  $\mathbf{E} \cdot \mathbf{B} \neq 0$ , where  $\mathbf{E}$  and  $\mathbf{B}$  are the electric and magnetic fields, was presented in Damour et al. (1978). These early results led to the definitions of the dyadosphere (Preparata et al. 1998) and dyadotorus (Cherubini et al. 2009) which served as the basis of the GRB acceleration process and consequently for their phenomenological interpretation (Ruffini et al. 2010).

This very successful approach did not address, at the time, the physical origin of the BH charge,  $Q$ , which was treated as an independent parameter.

The first attempt to extract energy from a Kerr BH, in absence of charge, by a plasma accreting onto it was presented in Ruffini & Wilson (1975). The infinite conductivity condition,  $F_{\mu\nu}U^\nu = 0$  was used there leading to the condition  $\mathbf{E} \cdot \mathbf{B} = 0$ . No process of energy extraction was possible there (Cherubini et al. 2018).

In parallel with this work on BHs, extensive research on the magnetosphere of pulsars, originating from a fast rotating NS, had been developed. The condition  $\mathbf{E} \cdot \mathbf{B} = 0$  also applies in the case of pulsars. In order to explain the observed pulsar radiation the existence of “gaps” close to the NS surface was introduced (Sturrock 1971; Ruderman & Sutherland 1975). This allowed the condition  $\mathbf{E} \cdot \mathbf{B} \neq 0$  to be satisfied, necessary for the initial particle acceleration to hold. The first acceleration of particles up to ultra-relativistic energies with Lorentz gamma factors of  $10^6$ – $10^7$  were assumed to occur in these “gaps”. The pulsar radiation was then explained by the deceleration of these particles by synchrotron radiation and their cascades in the fast rotating dipole magnetic field at large distances from the NS surface, close to the light cylinder,  $r = c/\omega$ , (Ruderman & Sutherland 1975; Daugherty & Harding 1982, 1983).

The idea of using the “gap” theory in order to accelerate particles in an accreting Kerr BH, overcoming the condition of  $\mathbf{E} \cdot \mathbf{B} = 0$ , was introduced by Blandford & Znajek (1977). They imposed on the Ruffini & Wilson (1975) solution a force-free condition,  $F_{\mu\nu}J^\nu = 0$ , and added the concept of “gaps” located outside the BH horizon. For more details about the force-free and infinite conductivity conditions, see Gralla & Jacobson (2014); Cherubini et al. (2018).

Wald (1974) had originally indicated that in his solution  $\mathbf{E} \cdot \mathbf{B} \neq 0$ . Miniutti & Ruffini (2000) derived the quadrupolar distribution of charges in the Wald solution and indicated that acceleration of particles along the field lines would occur near the horizon. The proposal

that this property of the Wald solution could be used as the basis of GRB energetic requirements was initially presented in Ruffini et al. (2018e). There it was shown that the presence of a magnetic field of  $\sim 10^{14}$  G aligned with the rotation axis of the BH can indeed 1) accelerate particles to ultrarelativistic energies of  $\sim 10^{21}$  eV and emit synchrotron radiation in the GeV and in the TeV, 2) that the high energy emission occurs in the elementary events of energy  $\sim 10^{44}$  erg on a timescale on the order of  $\sim 10^{-6}$  s, 3) that this energy extraction occurs at the expense of the rotational energy of the BH.

In this article we complete the analysis of the elementary events and address the fundamental issue of their temporal sequence occurring in GRB 130427A.

In this novel approach adopting the Wald solution, *no* “gaps” and *no* “charges” are needed:

1) protons are injected close to the horizon with an initial Lorentz gamma factor of  $\gamma = 1$ ; 2) they are monotonically accelerated by the electromagnetic field of the Wald solution all the way up to high energies also emitting synchrotron radiation, see Eq. (25) and section 5 and 3) the synchrotron radiation for various injection angles leads to GeV, TeV and PeV radiation on a time scale of  $10^{-6}$  s or equivalently within  $10^5$  cm from the BH horizon, see Eq. (36) and section 5 for details.

This novel approach overcomes the conceptual difficulty of explaining the origin of the charge,  $Q$ , in the BH electrodynamics. Indeed an effective charge is expressed as

$$Q_{\text{eff}} = \frac{B_0 J}{2M^2} r_+^2, \quad (3)$$

which is not an independent parameter but it is function of the BH mass and angular momentum and the magnetic field  $B_0$  of the Wald solution, which become the free parameters of the electrodynamic process in GRBs (Ruffini et al. 2018e). The concept of charge is no longer needed as a primary concept. The previous success of using the net charge (Ruffini et al. 2010), is explained in terms of Eq. 3

### 3. DETERMINATION OF THE MASS AND SPIN OF THE BH

In this section we identify the rotational energy of a Kerr BH as the energy source powering the GeV emission and consequently the mass and spin of the BH can be determined. We exemplify this in the case of GRB 130427A, see Fig. 2.

As detailed in Levan et al. (2013); von Kienlin (2013); Xu et al. (2013); Flores et al. (2013); Ruffini et al. (2015), with the exception of pile up encountered in the prompt emission, GRB 130427A records a well observed fluence

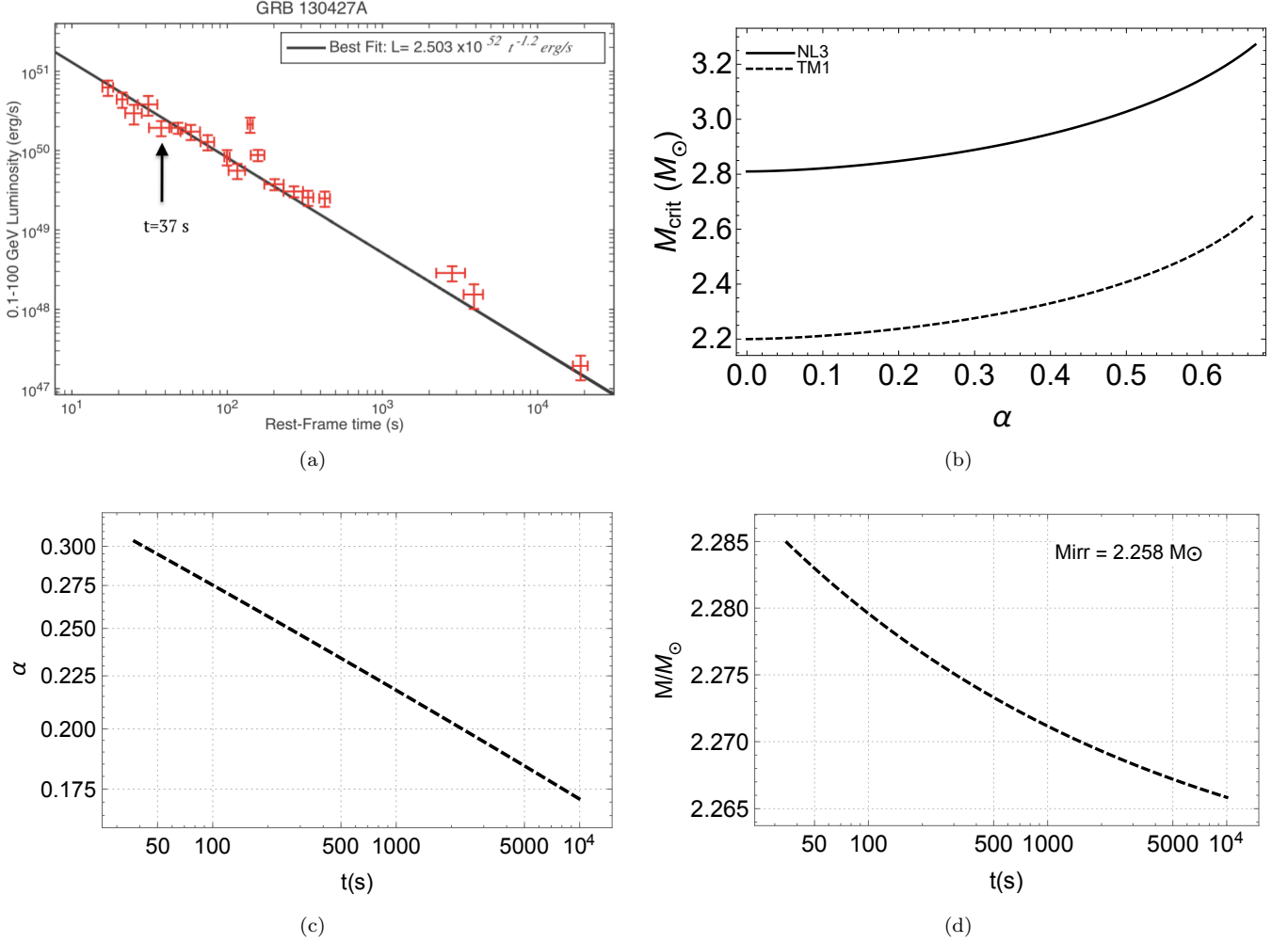


**Figure 3. a:** The rest-frame 0.1–100 GeV luminosity light-curve of GRB 130427A obtained from *Fermi*-LAT. The black line shows the best fit for power-law behavior of the GeV emission with slope of  $1.2 \pm 0.04$  and amplitude of  $2.053 \times 10^{52} \text{ erg s}^{-1}$ . **b:** NS critical mass as a function of the spin parameter  $\alpha$  for the NL3 and TM1 EOS. We recall that the maximum spin parameter of a uniformly rotating NS is  $\alpha_{\text{max}} \approx 0.71$ , independently of the NS EOS; see e.g. [Cipolletta et al. \(2015\)](#). **c and d:** The decrease of the BH spin and Mass, as a function of rest-frame time for GRB 130427A for TM1 EOS. The values of spin and mass at the moment which prompt is finished which has been assumed to occur at the rest-frame time of  $t_{\text{rf}} = 37.3 \text{ s}$ , are:  $\alpha = 0.303$  and  $M(\alpha) = 2.285 M_{\odot}$ .

in the optical, X-ray, gamma-ray and GeV bands after  $t_{\text{rf}} = 37 \text{ s}$ , see Fig. 2.

The 0.1–100 GeV-emission phase data obtained from *Fermi*-LAT together with the best fit of luminosity when measured in the rest-frame of the source,  $L_{\text{GeV}} = 2.503 \times 10^{52} (t/1\text{s})^{-1.2 \pm 0.04} \text{ erg s}^{-1}$  which has energy of  $E_{\text{GeV}} = (5.69 \pm 0.05) \times 10^{52} \text{ erg}$ , are shown in Fig. 3a.

We now verify that the energetics of the GeV radiation can be explained by the extractable energy of the Kerr BH, i.e.,

$$E_{\text{GeV}} = E_{\text{extr}} = (5.69 \pm 0.05) \times 10^{52} \text{ erg}, \quad (4)$$

where

$$E_{\text{extr}} = Mc^2 - M_{\text{irr}}c^2 = \left(1 - \sqrt{\frac{1 + \sqrt{1 - \alpha^2}}{2}}\right) Mc^2, \quad (5)$$

with  $M$  and  $M_{\text{irr}}$  the mass and the irreducible mass of the BH, respectively.

For determining  $M$  and  $\alpha$  we need an additional equation besides Eqs. (4) and (5).

Since in the BdHN I the BH is formed at the end of the hypercritical accretion, when the NS reaches its critical mass, the specific value of the NS critical mass has to be taken into account. Two possible equations of state (EOS) have been assumed for this purpose. For the NL3



TM1		NL3	
$\alpha$	$M(M_\odot)$	$\alpha$	$M(M_\odot)$
$0.303^{+0.001}_{-0.001}$	$2.285^{+0.0006}_{-0.0006}$	$0.273^{+0.001}_{-0.001}$	$2.845^{+0.0005}_{-0.0005}$

**Table 1.** The spin  $\alpha$  and mass  $M$  of the BH applying the TM1 and the NL3 EOS in the case of GRB 130427A.

and TM1 EOS the numerical value of the critical mass of a rotating NS is well fit by (Cipolletta et al. 2015)

$$M_{\text{crit}}(\alpha) = M_{\text{crit}}^{J=0}(1 + kj^p), \quad (6)$$

where  $k$  and  $p$  are EOS-dependent parameters,  $M_{\text{crit}}^{J=0}$  is the critical mass of a non-rotating NS and  $j$  is the dimensionless angular momentum parameter related to  $\alpha$  by

$$j \equiv \alpha(M_{\text{crit}}/M_\odot)^2. \quad (7)$$

Therefore, Eq. (7) is an implicit equation for the NS critical mass as a function of the spin parameter,  $\alpha$ , which can be solved numerically. We show in Fig. 3 b such a relation for the NL3 and TM1 EOS. The maximum spin parameter is independent of the EOS of a uniformly rotating NS and is  $\alpha_{\text{max}} \approx 0.7$ ; see Fig. 3b, see for more details Cipolletta et al. (2015). For the two EOS of NS, for each value of  $E_{\text{extr}}$  there are two corresponding solutions for  $M(\alpha)$  and  $\alpha$  which are listed in Table 1.

From the GeV luminosity expressed in the rest-frame of the source, we can determine the initial value of mass within the TM1 EOS is  $M_0 = 2.285M_\odot$  at  $t_{\text{rf}} = 37$  s; see Fig. 2. This initial mass leads to  $M_{\text{irr}} = 2.258M_\odot$ .

From the luminosity expressed in the rest-frame of the sources, and from the initial values of the spin and of the mass of the BH we can now derive the slowing down of the BH due to the energy loss in the GeV emission. The time derivative of Eq. (5) gives the luminosity

$$L = -\frac{dE_{\text{extr}}}{dt} = -\frac{dM}{dt}, \quad (8)$$

Since  $M_{\text{irr}}$  is constant for each BH during the energy emission process, and using our relation for luminosity

$$L = A t^{-1.2} = 2.503 \times 10^{52} (t/1\text{s})^{-1.2 \pm 0.04} \text{ erg s}^{-1} \quad (9)$$

we obtain the relation of the loss of mass-energy of the BH by integrating Eq. (8):

$$M = M_0 + 5At^{-0.2} - 5At_0^{-0.2}, \quad (10)$$

which  $M_0$  is the initial mass of the newborn BH. From the mass-energy formula of the BH we have

$$J = 2M_{\text{irr}} \sqrt{M^2 - M_{\text{irr}}^2}, \quad (11)$$

therefore

$$a = \frac{J}{M} = 2M_{\text{irr}} \sqrt{1 - \frac{M_{\text{irr}}^2}{(M_0 + 5At^{-0.2} - 5At_0^{-0.2})^2}}. \quad (12)$$

The behaviour of  $\alpha = J/M^2$  and  $M$  with time are shown in Fig. 3 c and Fig. 3 d. Both  $\alpha$  and  $M$  decrease with time which shows the decrease of rotational energy of the BH due to the energy loss in GeV radiation; see Fig. 3c and Fig. 3d.

#### 4. ON THE ELECTRODYNAMICS OF THE “INNER ENGINE”

Having established that the rotational energy of the Kerr BH can power the GeV emission, we turn now to the description of the electrodynamical mechanism in the *inner engine* which extracts the rotational energy.

In the following we focus on a Wald solution within a cone of opening angle  $\pi/3$  about the magnetic field direction, see Fig. 4. We address only the leading terms in the angle and radial dependence of the field in the equation of motion.

The electromagnetic field of the *inner engine*, in the first-order, slow rotation approximation,  $a/(GM/c) = cJ/(GM^2) \ll 1$ , and at second-order, small angle approximation, reads:

$$E_{\hat{r}} \approx -\frac{aB_0}{r} \left[ \left(1 + \frac{GM}{c^2 r}\right) \theta^2 - \frac{2GM}{c^2 r} \right], \quad (13)$$

$$E_{\hat{\theta}} \approx -\frac{aB_0}{r} \left(1 - \frac{2GM}{c^2 r}\right)^{1/2} \theta, \quad (14)$$

$$B_{\hat{r}} \approx -B_0 \left(1 - \frac{\theta^2}{2}\right), \quad (15)$$

$$B_{\hat{\theta}} \approx B_0 \left(1 - \frac{2GM}{c^2 r}\right)^{1/2} \theta, \quad (16)$$

where  $J$  and  $M$  are the angular momentum and mass of the BH and  $a = J/M$ .

Up to linear order in  $\theta$ , the radial component of the electric field can be approximated by the expression

$$E_r \approx \frac{B_0 J}{2GM^2} \frac{r_+^2}{r^2} c^2, \quad (17)$$

which has been shown to be accurate, within 5% of error with respect to the numerical values given by the full expression, for values  $\alpha \lesssim 0.7$  (see Ruffini et al. 2018e, for details).

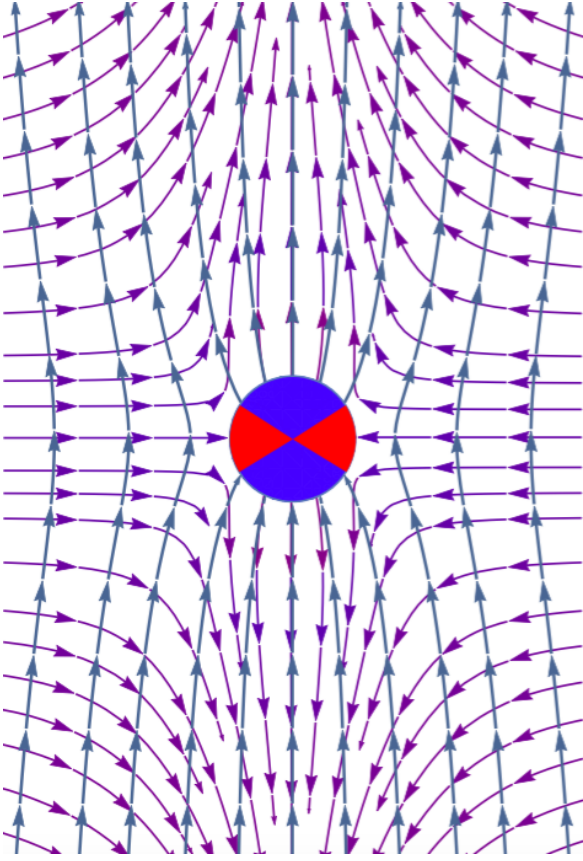


**Figure 4.** The electromagnetic field lines of the Wald solution. The blue lines show the magnetic field lines and the violet lines show the electric field lines. On the polar axis up to  $\theta \sim 60^\circ$  electric field lines are outwardly directed, therefore protons will be accelerated away from the BH. For  $\theta > 60^\circ$  electric field lines are inwardly directed and consequently electrons will be accelerated away from the BH.

At the BH horizon,  $r_+ = (1 + \sqrt{1 - \alpha^2})GM/c^2$ , the above electromagnetic field becomes

$$E_{\hat{r}} \approx \frac{aB_0c^2}{2GM} \left(1 - \frac{3}{2}\theta^2\right), \quad (18)$$

$$E_{\hat{\theta}} \approx 0, \quad (19)$$

$$B_{\hat{r}} \approx -B_0 \left(1 - \frac{\theta^2}{2}\right), \quad (20)$$

$$B_{\hat{\theta}} \approx 0, \quad (21)$$

where  $\alpha = (c/G)(a/M) = (c/G)(J/M^2)$  is the dimensionless angular momentum parameter. It can be seen from the full numerical solution keeping all orders in the angular momentum, shown in Fig. 4, that this approximation is valid up to  $55^\circ \lesssim \theta_{\pm} \lesssim 60^\circ$  and for arbitrary value of  $\alpha$  and within such limits our small angle approximation gives accurate qualitative and quantitative results.

We now recall the definition of the critical electric and magnetic fields,  $E_c$  and  $B_c$ , i.e.

$$E_c = \frac{m_e^2 c^3}{e\hbar}, \quad B_c = \frac{m_e^2 c^2}{e\hbar} \quad (22)$$

where  $m_e$  and  $e$  are the electron mass and charge, respectively. If the associated electric field is overcritical, a plasma consisting of a vast number of  $e^+e^-$  pairs is produced by the vacuum polarization process. Such a plasma by self-acceleration produces, interacting with the GeV radiation, the ultrarelativistic *prompt* emission phase (UPE) (Ruffini et al. 2019b). This case is presented in a forthcoming paper for GRB 190114C (Ruffini, et al., To be submitted).

In the present paper we impose following Ruffini et al. (2018e) the condition  $E \lesssim E_c$  to occur at  $T_{50}$  s of the GBM data, namely  $t_{\text{rf}}=37$  s, so overcoming the both the “pile up” problem in the GBM data and the description of the overcritical field, see Fig. 2. This case is more easily treated here qualitatively and quantitatively.

We show how in the presence of a fully ionized low-density plasma, the GRB *inner engine* accelerates protons up to ultrarelativistic energies in the above mentioned cavity.

We assume that the emission process occurs near the BH and within magnetic field lines of  $10^{14}$  G constant in time and uniform in space. The equations of motion for the protons injected for selected angles  $\theta$  are given below and specific examples in the section 5.

When emitted in the polar direction  $\theta = 0$ , the *inner engine* can give rise to UHECRs. For  $\theta \neq 0$  we integrate the equations of motion and evaluate the synchrotron emission keeping the leading terms.

## 5. SYNCHROTRON EMISSION FROM THE WALD SOLUTION AND THE FIRST ELEMENTARY IMPULSIVE EVENT

The relativistic expression for the Lorentz force is

$$\frac{dp^\mu}{d\tau} = \frac{e}{c} F^{\mu\nu} u_\nu, \quad p^\mu = m u^\mu, \quad u^\mu = \frac{dx^\mu}{d\tau}, \quad (23)$$

where  $\tau$  is the proper time,  $p^\mu$  is the four-momentum,  $u^\mu$  is the four-velocity,  $x^\mu$  are the coordinates,  $F^{\mu\nu}$  is the electromagnetic field tensor,  $m$  is the particle mass,  $e$  is the elementary charge and  $c$  is the speed of light. This expression can be rewritten in the laboratory frame using vector notation as

$$mc \frac{d(\gamma \mathbf{v})}{dt} = e (\mathbf{E} + \mathbf{v} \times \mathbf{B}). \quad (24)$$

Assuming the one-dimensional motion along the radial directions, the dynamics of the protons in the electro-

magnetic field (18)-(21), for  $\gamma \gg 1$ , is determined by the equation (see, e.g., de Jager et al. 1996)

$$m_p c^2 \frac{d\gamma}{dt} = e \frac{B_0 J}{2GM^2} c^2 - \frac{2}{3} e^4 \frac{B_0^2 \sin^2 \langle \theta \rangle}{m_p^2 c^3} \gamma^2 c^2, \quad (25)$$

where  $\gamma$  is the proton Lorentz factor,  $\langle \theta \rangle$  is the injection angle between the direction of proton motion and the magnetic field and  $m_p$  is the proton mass. This equation is here integrated for protons assumed to be injected near the horizon, for selected value of the injection angle  $\langle \theta \rangle$ , with an initial Lorentz factor of  $\gamma = 1$  at  $t = 0$ .

Equation (25) is valid for every injection angle  $\theta$ . The angle dependence in the electric field in Eq. (25) is neglected since the second term of the right-hand side of Eq. (25), namely the synchrotron radiation term, is largely dominant for the parameters of interest in this work.

Assuming all parameters are constant, the approximate solution in the limit  $\gamma \gg 1$  is

$$\gamma = \gamma_{\max, p} \tanh \left[ \frac{2}{3} \frac{e^2}{\hbar c} \left( \frac{B_0 \sin \langle \theta \rangle}{B_c} \right)^2 \left( \frac{m_e}{m_p} \right)^2 \gamma_{\max, p} \frac{t}{\hbar/m_e c^2} \right], \quad (26)$$

which has the following asymptotic value:

$$\gamma = \begin{cases} \frac{1}{2} \frac{m_e}{m_p} \frac{B_0}{B_c} \alpha \frac{t}{\hbar/m_e c^2}, & t \ll t_c, \\ \gamma_{\max, p}, & t \gg t_c, \end{cases} \quad (27)$$

where

$$\gamma_{\max, p} = \frac{1}{2} \left( \frac{3}{\frac{e^2}{\hbar c}} \alpha \frac{B_c}{B_0 \sin^2 \langle \theta \rangle} \right)^{1/2} \frac{m_p}{m_e}, \quad (28)$$

and the critical time is

$$t_c = \frac{\hbar}{m_e c^2} \frac{3}{\sin \langle \theta \rangle} \left( \frac{m_e}{m_p} \right)^{-2} \left[ \frac{e^2}{\hbar c} \left( \frac{B_0}{B_c} \right)^3 \alpha \right]^{-1/2}. \quad (29)$$

The maximum energy of photons emitted by the proton-synchrotron mechanism is obtained from the equilibrium between energy gain and energy loss in Eq. (25). Consequently, the following maximum energy of the proton-synchrotron photons is found:

$$\begin{aligned} \epsilon_{\max, \gamma} &= \frac{3e\hbar}{2m_p c} B_0 \sin \langle \theta \rangle \gamma_{\max, p}^2 = \frac{9}{2} \epsilon \frac{m_p c^2}{e^2 / \hbar c \sin \langle \theta \rangle} \alpha \\ &\approx \frac{144}{\sin \langle \theta \rangle} \alpha \text{ GeV}. \end{aligned} \quad (30)$$

The maximum energy is independent of the magnetic field strength, which for different angles leads to different

energy bands for the photons; see Fig. 5. From this upper limit some inferences on the TeV emission are in preparation, awaiting the publication of the TeV data. Here we return to the GeV emission and to its energy originating from the BH rotational energy.

A vast literature exists on the propagation of ultra high energy protons in a magnetic field with  $\theta = \pi/2$  (see e.g., Erber 1966, and references therein). Very little has been published for computations for small injection angles,  $\theta \approx 0$  (an important exception being Harding 1991) which we here address.

Having determined the values of the spin and of the mass of the BH,  $\alpha = 0.303$  and  $M(\alpha) = 2.285 M_\odot$  at  $t_{\text{rf}} = 37$  s (see Sec. 3 and Fig. 2), and having formulated the electrodynamical equations we assume at the starting time of the first elementary impulsive event, that the electric field of Eq. (17) at the horizon must satisfy  $E_{r_+} = E_c$ . We consequently determine the magnetic field  $\beta = B_0/B_c = 6.7$ . We also assume that the magnetic field  $\beta$  remains constant during the radiation processes (Ruffini et al. 2018c).

Having obtained the value of  $B_0$ , we can now integrate the equation of motion of the accelerated protons as a function of  $\theta$ .

The electric potential difference associated with the electric field given by Eq. (17) is

$$\begin{aligned} \Delta\phi &= \frac{\epsilon_p}{e} = \int_{r_+}^{\infty} E dr = E_{r_+} r_+ \\ &= 9.7 \times 10^{20} \cdot \xi \beta \mu (1 + \sqrt{1 - \xi^2}) \frac{\text{eV}}{e}, \end{aligned} \quad (31)$$

which can accelerate protons along the symmetry axis,  $\theta = 0$ , to Lorentz factors  $\gamma_p = \epsilon_p/(m_p c^2) \sim 10^{12}$  (Ruffini et al. 2018e). Therefore, the proton energies can reach values  $\epsilon_p = \gamma_p m_p c^2 \sim 10^{21}$  eV.

For  $\theta \neq 0$ , we integrate the equation of motion given by Eq. (25). As an example we show the proton propagation for selected angles, i.e.,  $\theta = \pi/3$ ,  $\theta = 4.3 \times 10^{-2}$ ,  $\theta = 4.3 \times 10^{-5}$ ,  $\theta = 4.3 \times 10^{-8}$  and  $\theta = 3.7 \times 10^{-9}$  with respect to the direction of the magnetic field. The numerical solution of Eq. (25) along with analytic solutions are represented in Fig. 5a. The proton synchrotron luminosity from the right-hand side of Eq. (25) is

$$\dot{E}_{\text{synch}} = \frac{2}{3} e^4 \frac{B_0^2 \sin^2 \langle \theta \rangle}{m_p^2 c^3} \gamma^2. \quad (32)$$

In Fig. 5c we present the total power of the synchrotron emission by a single proton as a function of time, for injected angles  $\theta$ . The power increases with time and then at  $t > t_c$  approaches a constant value, which does not depend on the angle

$$\dot{E}_{\text{synch}, \gamma_{\max}} = \frac{1}{2} m_e c^2 \frac{B_0}{B_c} \alpha = 6.4 \times 10^{14} \text{ erg s}^{-1}. \quad (33)$$



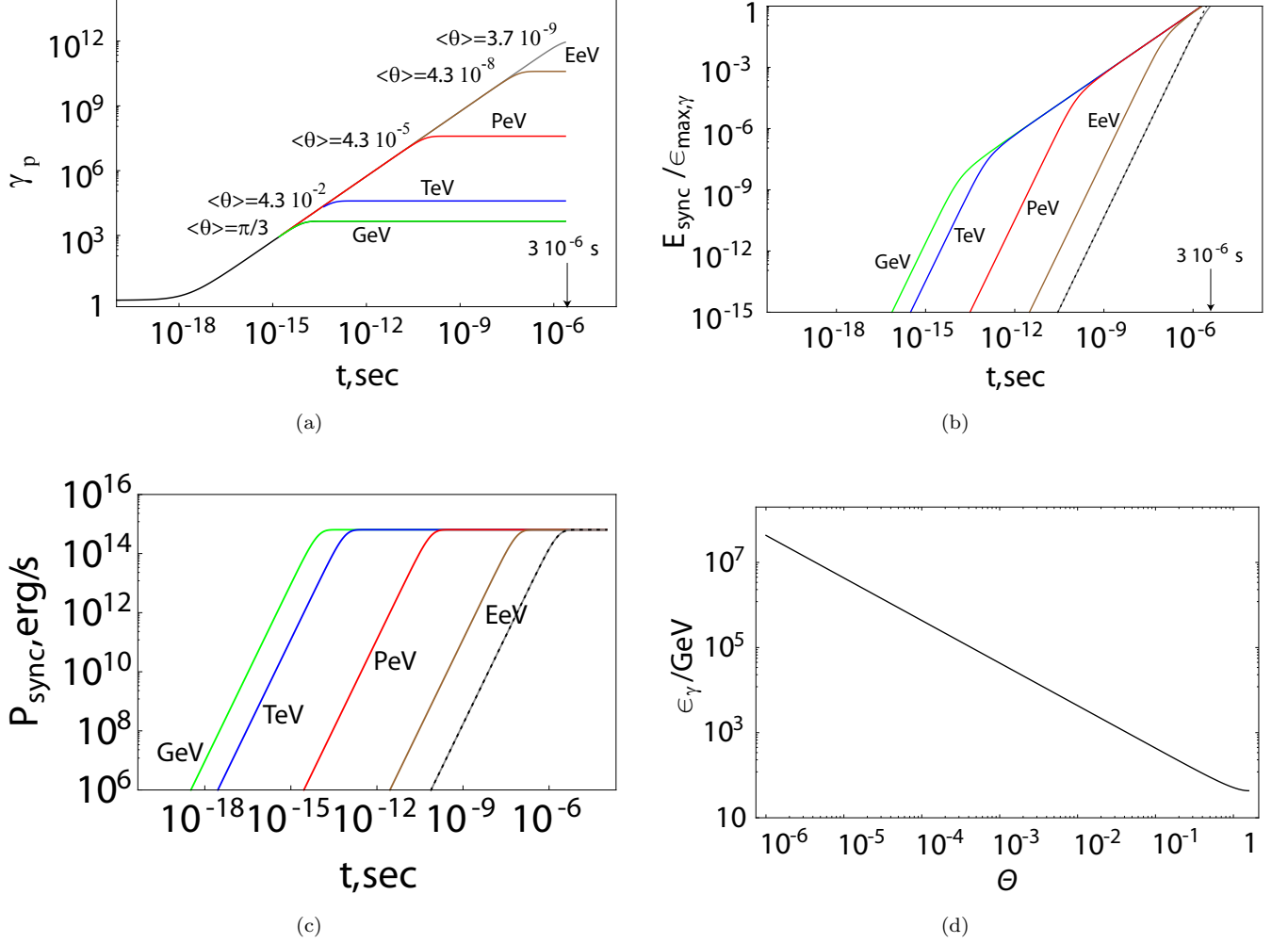


**Figure 5.** **a:** The proton Lorentz gamma factor obtained from solutions of Eq. (25) as functions of time: numerical (black), and analytic for selected angles:  $\theta = \pi/3$  (green),  $\theta = 4.3 \times 10^{-2}$  (blue),  $\theta = 4.3 \times 10^{-5}$  (red),  $\theta = 4.3 \times 10^{-8}$  (brown) and  $\theta = 3.7 \times 10^{-9}$  (grey). Parameters assumed:  $a/M = 0.3$ ,  $B_0/B_c = 6.7$  and  $E = E_C$ . The arrow indicates the time when the energy emitted in synchrotron radiation equals  $\epsilon_{\text{max}, \gamma} = 10^{21}$  eV, which is  $3.0 \times 10^{-6}$  s which is in agreement with timescale of the first *impulsive event*. **b:** Total energy emitted in synchrotron radiation from Eq. (34) as a function of time for selected angles given in Fig. 5(a). **c:** Power of synchrotron emission by a single proton as a function of time for selected angles given in Fig. 5(a). The dotted line corresponds to the second line in Eq. (34). **d:** Peak energy of synchrotron photons as a function of the angle between the proton velocity and the magnetic field.

In Fig. 5d we show the peak energy of the synchrotron photons as a function of the proton injection angle and the magnetic field.

The total energy emitted in synchrotron radiation, computed by integrating the synchrotron luminosity with time gives

$$E_{\text{sync}} = \begin{cases} \frac{1}{18} \frac{e^2}{\hbar c} \left( \frac{B_0}{B_c} \right)^4 \alpha^2 \left( \frac{m_e}{m_p} \right)^3 \left( \frac{t}{\hbar/m_e c^2} \right)^3 \sin^2 \langle \theta \rangle m_p c^2, & t \ll t_c, \\ \frac{1}{2} \alpha \frac{B_0}{B_c} \frac{m_e}{m_p} \frac{t}{\hbar/m_e c^2} m_p c^2, & t \gg t_c, \end{cases} \quad (34)$$

where from Eq. (29) the critical time for  $\alpha = 0.3$ ,  $B_0/B_c = 6.7$  is

$$t_c \simeq \frac{2.4 \times 10^{-14}}{\sin \langle \theta \rangle} \text{ s}. \quad (35)$$

Assuming the total energy available for the acceleration and radiation of each proton is  $\epsilon_p = 10^{21}$  eV, which is the total electrostatic energy available for one proton, the time when the radiated energy becomes equal to  $\epsilon_p$  is

$$\tau_{\text{th}} = \frac{\hbar}{m_e c^2} \frac{m_p}{m_e} \frac{10^{21} \text{ eV}}{\frac{\alpha}{2} \frac{B_0}{B_c}} = 3 \times 10^{-6} \text{ s}. \quad (36)$$

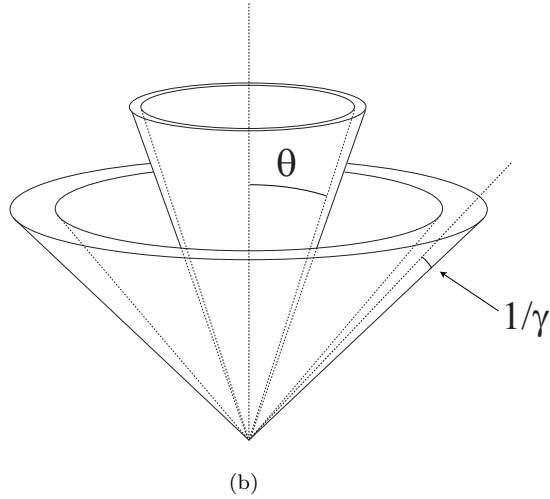
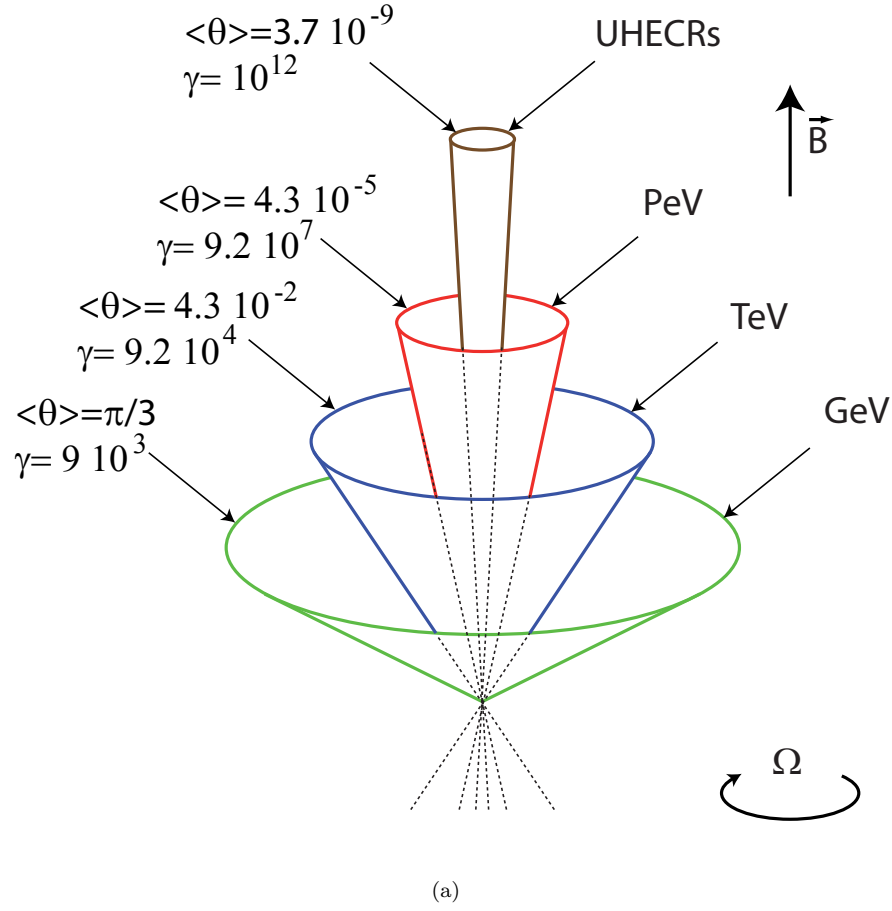


**Figure 6.** (Not to scale) **a:** Having evaluated the values of spin and magnetic field,  $a/M = 0.3$ ,  $B_0/B_c = 6.7$ , from Eq. (30) for selected injection angles we obtain the radiation in the different bands GeV, TeV and PeV. Using Eq. (30) we obtain that the maximum energy  $\epsilon_p = 10^{21}$  eV is reached at the angle  $\langle\theta\rangle = 3.7 \times 10^{-9}$ . This angle is an absolute lower limit for emitting synchrotron radiation, therefore for  $\langle\theta\rangle < 3.7 \times 10^{-9}$ , protons are accelerated to give rise to UHECRs. In this figure the magnetic field is “antiparallel” to the Kerr BH rotation axis and protons are accelerated outward and electrons captured by the horizon. **b:** Synchrotron emission from protons with pitch angle  $\theta$ . Radiation is concentrated in a cone of angle of  $1/\gamma$ .

This timescale, which is independent of  $\theta$ , leads to the conclusion that the acceleration of protons occurs within a radius of  $r = c \times \tau_{\text{th}} \sim 10^5$  cm from the BH, see Fig. 5b.

Following our previous work (Ruffini et al. 2018e) the electrostatic energy available is

$$\mathcal{E} = \frac{1}{2} E_{r_+}^2 r_+^3 = 7.5 \times 10^{41} \cdot \alpha^2 \beta^2 \mu^3 (1 + \sqrt{1 - \alpha^2})^3 \text{ erg}, \quad (37)$$

where  $E_{r_+}$  is the electric field evaluated at the horizon which for the *first elementary impulsive event* at  $t_{\text{rf}} = 37$  s gives

$$\mathcal{E}_1 \approx 2.75 \times 10^{44} \text{ erg}. \quad (38)$$

With this electromagnetic energy budget the system can accelerate a total number of protons  $N_p = \mathcal{E}_1 / \epsilon_p \approx 1.94 \times 10^{34}$ . Therefore, the timescale of the first impulsive event from the observed GeV luminosity is

$$\tau_{\text{ob},1} = \frac{\mathcal{E}_1}{L_{\text{GeV}}} = 1.17 \times 10^{-6} \text{ s}. \quad (39)$$

The timescale  $\tau_{\text{ob}}$  of the first *impulsive event* as evaluated from the GeV luminosity occurring at  $t_{\text{rf}} = 37$  s is in a good agreement with the synchrotron timescale,  $\tau_{\text{th}}$ , derived from the theory in Eq. (36).

In summary having obtained the values of spin,  $a/M = 0.3$ , and magnetic field,  $B_0/B_c = 6.7$ , from Eq. (30) we obtain the radiation in the GeV, TeV and PeV bands corresponding to selected values of  $\theta$ . Using Eq. (30) the maximum energy  $\epsilon_p = 10^{21}$  eV is reached at the critical angle  $\langle \theta \rangle = 3.7 \times 10^{-9}$ . This gives an absolute lower limit on the  $\langle \theta \rangle$  value for emitting synchrotron radiation. For  $\langle \theta \rangle$  smaller than this critical angle only UHECRs are emitted. See Fig. 5a and Fig. 6.

The timescale of the process is in general set by the density of particles around the BH, which is provided by the structure of the cavity and SN ejecta, see section 5.

We have already shown that during each such elementary process the BH experiences a very small fractional change of angular momentum (Ruffini et al. 2018e)

$$\begin{aligned} |\Delta J|/J &\approx (|\dot{J}|/J) \Delta t_{\text{el}} \approx 10^{-10}, \\ |\Delta M|/M &\approx (|\dot{M}|/M) \Delta t_{\text{el}} \approx 10^{-10}. \end{aligned} \quad (40)$$

The repetition time,  $\tau_{\text{ob}}$ , is determined by the density of the particles around the BH and itself determines the rate of the rotational energy loss of the BH which jointly generates the observed power-law behavior of the luminosity shown in Sec. 3 (see Fig. 3a).

The electromagnetic energy of the first impulsive event given above is a small fraction of total extractable

rotational energy of the Kerr BH, see Eq. (4):

$$\frac{\mathcal{E}_1}{E_{\text{ext}}} \approx 10^{-9}. \quad (41)$$

This clearly indicates that the rotational energy extraction from Kerr BH:

- 1) Occurs in “discrete quantized steps”.
- 2) Temporally separated by  $10^{-6}$  s.
- 3) The luminosity of the GeV emission in GRB 130427A is not describable by a continuous function as traditionally assumed: it occurs in a “discrete sequence of elementary quantized events” (Rueda and Ruffini in preparation).

There are three main conclusions which can be inferred from the theory of synchrotron radiation implemented in this section:

1. Synchrotron radiation is not emitted isotropically and is angle dependent, the smaller the angle the higher the synchrotron photon energy, see Eq. (30) and Fig. 6.
2. The energy emitted in synchrotron radiation before reaching its asymptotic value is a function of injection angle  $\theta$ , see first line of Eq. (34) and Fig. 5b.
3. The time scale of the synchrotron radiation corresponding to radiated energy of  $10^{21}$  eV is independent of  $\theta$  and for GeV, MeV, TeV and PeV the time of radiations is given by  $\sim 10^{-6}$  s, see Eq. (36).

In order to compare and contrast the results based on this essential theoretical treatment with observation we need to determine 1) the number of protons for each selected injection angle  $\theta$  and 2) to verify that the maximum radiated synchrotron energy is compatible with the electrostatic energy of  $10^{21}$  eV for each proton. 3) Taking to due account the role of the beaming angle which we have here derived, see Fig. 6.

## 6. THE REPETITION TIME OF SEQUENCE OF DISCRETE “ELEMENTARY IMPULSIVE EVENT”

We now finally study the sequence of iterative *impulsive events* in which the system starts over, with a new value of the electric field set by the new values of the BH angular momentum and mass,  $J = J_0 - \Delta J$  and  $M = M_0 - \Delta M$ , keeping the magnetic field value constant  $B_0$ .

We infer from the observed luminosity the evolution of the timescale  $\tau_{\text{ob}}(t)$  of the repetition time of the *impulsive events* by requiring it to explain the GeV emission, i.e.:

$$L_{\text{GeV}} = \frac{\mathcal{E}}{\tau_{\text{ob}}(t)}, \quad (42)$$

where  $\mathcal{E}$  is electrostatic energy. Therefore we obtain for the timescale

$$\tau_{\text{ob}}(t) = \frac{1}{2} \frac{E_{r_+}^2 r_+^3}{L_{\text{GeV}}}, \quad (43)$$

where  $E_{r_+}$  is the electric field evaluated at the horizon determined from the new values of  $J$  and  $M$ . Fig. 7 shows that  $\tau_{\text{ob}}$  is a monotonically increasing function of time.

The observed linear dependence can be understood as follows. The electric field goes as  $E_{r_+} \propto \alpha$  and  $\alpha \propto t^{-0.1}$  while  $r_+$  and  $M$  are very slowly varying functions of  $t$ , i.e., they remain nearly constant with respect to the change of  $\alpha$ , and  $L_{\text{GeV}} \propto t^{-1.2}$ . Then one obtains

$$\tau_{\text{ob}} \propto \frac{\alpha^2}{L_{\text{GeV}}} \propto \frac{t^{-0.2}}{t^{-1.2}} = t. \quad (44)$$

We identify the timescale  $\tau_{\text{ob}}$  with the repetition time of the impulsive event. The efficiency of the system diminishes with time, as shown by the increasing value of  $\tau_{\text{ob}}$  (see Fig. 7a). This can be understood by the evolution of the SN remnant (the circumburst, ionized medium). Namely, the density of particles near the BH decreases owing to the expansion of the remnant, making the iterative process become less efficient. As we have mentioned in the immediate vicinity of the BH a cavity is created of approximate radius  $10^{11}$  cm and with very low density on the order of  $10^{-13}$  g cm $^{-3}$  (Ruffini et al. 2019a). This implies an approximate number of  $6 \times 10^{44}$  protons inside the cavity. Then, the protons of the cavity can power the iterative process only for a short time of 1–100 s. We notice that at the beginning of the gamma-ray emission the required number of protons per unit time for the explanation of the prompt and the GeV emission can be as large as  $10^{42}$ – $10^{44}$  s $^{-1}$ . This confirms that this iterative process has to be sustained by the protons of the remnant, at  $r \gtrsim 10^{11}$  cm, which are brought from there into the region of low density and then into the BH.

We turn back now to give a leading order estimate of the timescale. For this we can make use of the Maxwell equations. After some manipulation and simplification, we can write the time evolution of the electric field at the BH horizon,  $E_{r_+}$ , as

$$\frac{d^2 E_{r_+}(t)}{dt^2} = -4\pi \frac{dJ_m(t, r_+)}{dt} = 4\pi e \cdot c \cdot \frac{\partial n(t, r_+)}{\partial t}, \quad (45)$$

where  $J_m = -e \cdot c \cdot n(t, r)$  is current density of inflowing particles and  $dn/dt$  the particle rate.

At the moment of the SN explosion the CO $_{\text{core}}$  outer layers (the ejecta) start a spherically symmetric expansion and follow an approximate power-law profile (Becerra et al. 2016)

$$n(t_0, r) = n_0 \left( \frac{r_0}{r} \right)^m, \quad (46)$$

with the index  $m \approx 2.7$ . The expansion is homologous,  $v = r/t$ . However, the presence of the NS companion

and the hypercritical accretion process onto it makes the distribution of SN matter become asymmetric (see e.g., Fig. 1 and Becerra et al. 2016, 2019) and changes the initial power-law profile. Centered on the BH, the density can be also approximated by a power-law profile like (46). Fig. 7b shows the density profiles along selected directions on the equatorial plane where the angle  $\theta = 0$  describes the line joining the centers of the  $\nu$ NS and the newly born BH. The BH is located at the origin (0, 0).

Therefore, the density at a fixed position  $r$  (from the BH) decreases as:

$$n(t, r) = n(t_0, r) \left( \frac{t}{t_0} \right)^{-3+m}, \quad (47)$$

which implies  $\dot{n}(t, r) = -(3 - m)n(t, r)/t$ , and then  $\dot{J}_m(t, r) = -e \cdot c \cdot (m - 3) \cdot n(t, r)/t \propto t^{-4+m}$ .

Equation (45) can be solved for  $\tau$  by introducing  $E_{r_+} = E_0 e^{-t/\tau}$ , and then evaluating the density at the innermost layer  $r_0$  we obtain:

$$\tau(t) = k t^{(4-m)/2}, \quad k = \left( \frac{1}{3} \frac{n_+}{n_0} \frac{T_+}{t_0^{3-m}} \right)^{1/2}, \quad (48)$$

where we have introduced:  $n_+ = 3N_p/(4\pi r_+^3)$  and  $T_+ = r_+/c$ . Adopting  $n \propto r^{-2}$  around the BH, Eq. (48) leads to  $\tau = kt$ . By using  $t_0 = 10$  s and  $n_0 \sim 3 \times 10^{25}$  cm $^{-3}$ , corresponding to a density  $10^2$  g cm $^{-3}$  of ionized matter near the BH as obtained from our 3D-SPH numerical simulations (see Fig. 7b), we obtain  $k \approx 2 \times 10^{-8}$ , in agreement with the value  $k \approx 3 \times 10^{-8}$  obtained from the GeV emission data (see Fig. 7a).

We are currently examining the operational condition of the inner engine in the cavity and in the circumburst medium acquiring the necessary data in the GeV, TeV, PeV and UHECR regimes (Ruffini et al. in preparation).

## 7. PRELIMINARY INFERENCES FROM THE OBSERVATION OF GRB 190114C

1. While revising this article, many important results have appeared from the preliminary analysis of the GRB 190114C: from the detailed time-resolved spectral analysis of the prompt radiation we have been able to verify by observation and confirm some of the expected features of BdHN. The SN shock breakout, the formation of the BH and the onset of the GeV emission, as well as the existence of the cavity already announced in this article have been confirmed (Ruffini et al. 2019b); (Liang Li et al., 2019 to be submitted).

2. What was totally unexpected has been the observation of self-similarities in the ultrarelativistic prompt emission phase (UPE) lasting for 2 s, see Ruffini et al. (2019a,b). For the comprehension of these observations

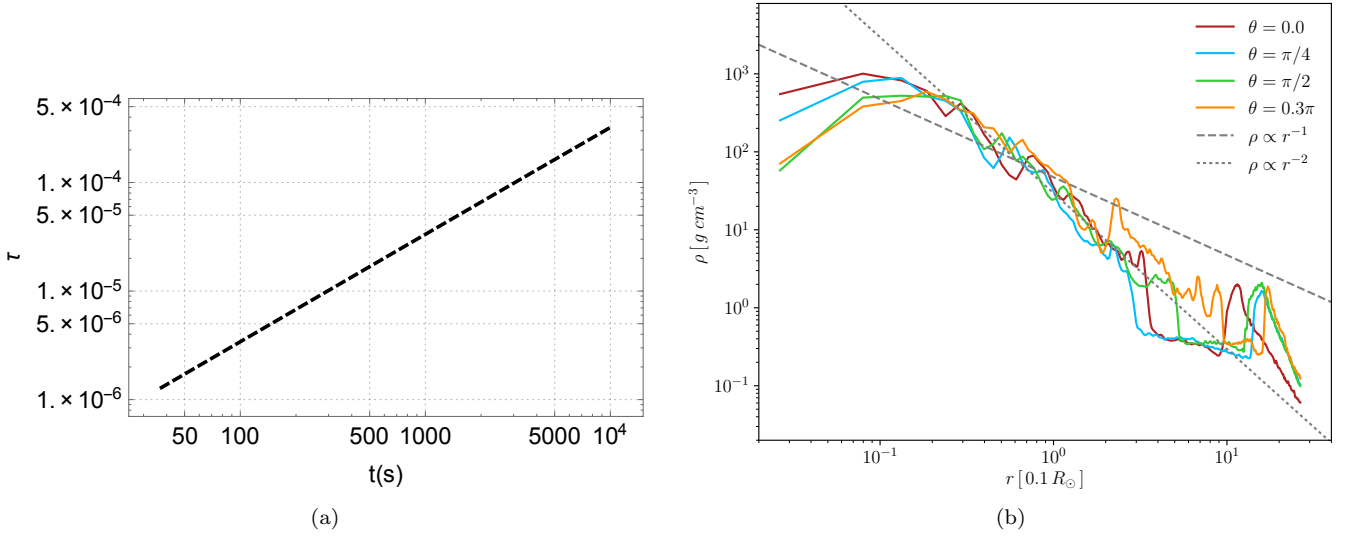


**Figure 7.** (a): The value of  $\tau_{\text{ob}}(t) = E_{r+}^2 r_+^3 / (2L_{\text{GeV}})$  calculated from the GeV luminosity data obtained from *Fermi*-LAT together with the values of  $E_{r+}$  and  $r_+$  obtained from the Wald field in each *impulsive event*. The timescale  $\tau(t)$  increases linearly with the time  $t$  (in seconds) with a slope  $\approx 3 \times 10^{-8}$ . (b): Density profile along selected directions in the equatorial plane  $x$ - $y$ , around the newly born BH (see Fig. 1) located at the position  $(0,0)$ . Here  $\theta$  measures the counterclockwise angle with respect to the line joining the center of the  $\nu$ NS and the newly born BH. The dotted and dashed lines correspond to the power-laws  $r^{-2}$  and  $r^{-1}$ , respectively.

the discrete quantized nature of the GeV emission first introduced in this article is essential. It is remarkable that these properties have been already confirmed in GRBs 090926A, 160509A and 160625B in Liang Li et al., 2019 (to be submitted).

3. Much has been learned from the observation of the afterglow of GRB 190114C, see Rueda et al. (2019). There evidence is given that the uniform and constant magnetic field in the Wald solution originates during the hypercritical accretion process of the hypernova on the companion NS. Simulations by Wilson (1978); Rezzolla et al. (2011); Dionysopoulou et al. (2013); Nathanail et al. (2017); Most et al. (2018) give evidence that the uniform magnetic field up to the  $10^5$  cm from the horizon, where the synchrotron radiation originates, develops a dipolar structure at large distance.

The flux of GeV photons is much higher than the flux of soft photons in the cavity in GRB 190114C (Ruffini et al. 2019a), so GeV photons are hydrodynamically dominant and hence propagate through the cavity without losses. Also the magnetic field is self-regulated by electromagnetic cascades creating the condition of transparency allowing the GeV radiation to escape.

For each synchrotron photon propagating in the magnetosphere a cascade will develop and it will be necessary to trace the conclusion of these cascades when the lower energy photons can escape without pair production. In addition to the energy degradation, the rapid decrease of the field strength, mentioned above, is also

instrumental in ending the cascades (Daugherty & Harding 1982).

For GRB 190114C, at  $z = 0.42$  an additional transparency condition has to be fulfilled for the TeV radiation observed by MAGIC (Mirzoyan et al. 2019). The absorption by extragalactic background light (EBL) cut-off has to be addressed (Ruffini et al. 2016a).

The transparency condition cannot be determined simply out of first principles. A vigorous interaction between theory and observation will be needed in order to fulfill the transparency condition of observed radiation in MeV (Fermi-GBM), GeV (Fermi-LAT) and TeV (MAGIC) energy bands.

## 8. CONCLUSIONS

In a previous article (Ruffini et al. 2018e) we have shown that the *inner engine* of a type I BdHN is composed of a uniform magnetic field of approximately  $10^{14}$  G aligned with the rotation axis of a Kerr BH, as described by the Wald solution (Wald 1974). There the case of the single, first impulse was analyzed. It was shown that protons along the rotation axis are accelerated to energies which can explain the UHECRs.

In this article:

1. We show the sequence of elementary impulses and have determined their recurrence times.
2. We have shown that the recurrence time starts from  $10^{-6}$  s and slowly increases linearly with time, see Eq. (39) and Fig. 7.



3. We then demonstrate that such a qualitative and quantitative behavior of the elementary process timescale is explained by the decrease of the density around the BH due to the creation of the cavity (Ruffini et al. 2019a) and the nearly homologous expansion of the ejecta.

Turning to the specific operation of the “*inner engine*” leading to the emission of the GeV, TeV and PeV radiation; see Fig. 5 and Fig. 6, we can conclude that:

a. The emission region of synchrotron radiation by protons, accelerated to ultrarelativistic energies, originates in a uniform magnetic field of  $10^{14}$  G in a region of  $10^5$  cm close to the BH horizon. The magnetic field is expected to decrease at larger distance reaching a dipolar structure.

b. The acceleration time up to the final synchrotron emission is  $\tau_{\text{th}} = 3 \times 10^{-6}$  s independent of the angle of injection in the uniform magnetic field. This is in agreement with the repetition time of  $\tau_{\text{ob}}$  derived from the *inner engine* and observed luminosity; see Eqs. (39) and (43).

c. The electromagnetic energy emitted in each single elementary event is  $\sim 10^9$  times smaller than the BH rotational energy, which guarantees that the extraction of the BH rotational energy via this electromagnetic process lasts for thousands of years.

As an overall conclusion the energy emission per proton in this electrodynamically dominated *inner engine* is  $10^{15}$  times larger than the one expected in gravitational accretion process around a Kerr BH.

We are currently extending the analysis presented in this article to the AGN IC 310 as well as M87, where

the GeV-TeV emission from the horizon is not only an option but is mandatory in view of the observed time variability on purported subhorizon scales (Aleksić et al. 2014).

Having reached a deeper understanding of the elementary impulsive event presented in Ruffini et al. (2018e), as well as having developed here the treatment of the sequence of impulsive events made possible by the excellent LAT data for GRB 130427A, we now address the new astrophysical scenario made possible by the excellent GBM data of GRB 190114C including the recently discovered self-similarities and power-laws in GRB 190114C (Ruffini et al. 2019b) and GRBs 090926A, 160509A and 160625B in Liang Li et al., 2019 (to be submitted). Both these results point to the existence of “a quantum” underlining the GRB and the AGN astrophysics (Rueda & Ruffini; to be submitted).

We thank the Referee for the detailed reports and precise questions which have motivated a more precise formulation of our paper. We are grateful to Prof. G. V. Vereshchagin and to S. Campion for discussions in formulating the synchrotron radiation considerations and the related figures in the revised version. M.K. is supported by the Erasmus Mundus Joint Doctorate Program Grant N.2014–0707 from EACEA of the European Commission. N.S. acknowledges the support of the RA MES State Committee of Science, in the framework of the research project No. 18T-1C335.

## REFERENCES

- Ackermann, M., Ajello, M., Asano, K., et al. 2014, *Science*, 343, 42
- Aleksić, J., Ansoldi, S., Antonelli, L. A., et al. 2014, *Science*, 346, 1080
- Becerra, L., Bianco, C. L., Fryer, C. L., Rueda, J. A., & Ruffini, R. 2016, *ApJ*, 833, 107
- Becerra, L., Ellinger, C. L., Fryer, C. L., Rueda, J. A., & Ruffini, R. 2019, *ApJ*, 871, 14
- Becerra, L., Guzzo, M. M., Rossi-Torres, F., et al. 2018, *ApJ*, 852, 120
- Blandford, R. D., & Znajek, R. L. 1977, *MNRAS*, 179, 433
- Cherubini, C., Filippi, S., Loppini, A., et al. 2018, *Phys. Rev.*, D97, 064038
- Cherubini, C., Geralico, A., Rueda, H. J. A., & Ruffini, R. 2009, *PhRvD*, 79, 124002
- Christodoulou, D. 1970, *PhRvL*, 25, 1596
- Christodoulou, D., & Ruffini, R. 1971, *PhRvD*, 4, 3552
- Cipolletta, F., Cherubini, C., Filippi, S., Rueda, J. A., & Ruffini, R. 2015, *PhRvD*, 92, 023007
- Damour, T., Hanni, R. S., Ruffini, R., & Wilson, J. R. 1978, *Phys. Rev. D*, 17, 1518
- Damour, T., & Ruffini, R. 1975, *PhRvL*, 35, 463
- Daugherty, J. K., & Harding, A. K. 1982, *ApJ*, 252, 337
- . 1983, *ApJ*, 273, 761
- de Jager, O. C., Harding, A. K., Michelson, P. F., et al. 1996, *ApJ*, 457, 253
- Dionysopoulou, K., Alic, D., Palenzuela, C., Rezzolla, L., & Giacomazzo, B. 2013, *PhRvD*, 88, 044020
- Erber, T. 1966, *Reviews of Modern Physics*, 38, 626
- Flores, H., Covino, S., Xu, D., et al. 2013, *GCN Circ.*, 14491
- Gibbons, G. W., Mujtaba, A. H., & Pope, C. N. 2013, *Classical and Quantum Gravity*, 30, 125008

- Gralla, S. E., & Jacobson, T. 2014, MNRAS, 445, 2500
- Harding, A. K. 1991, Science, 251, 1033
- Hawking, S. W. 1971, Physical Review Letters, 26, 1344
- Levan, A. J., Cenko, S. B., Perley, D. A., & Tanvir, N. R. 2013, GCN Circ., 14455
- Miniutti, G., & Ruffini, R. 2000, Nuovo Cimento B Serie, 115, 751
- Mirzoyan, R., Noda, K., Moretti, E., et al. 2019, GCN Circ., 23701
- Most, E. R., Nathanail, A., & Rezzolla, L. 2018, ApJ, 864, 117
- Nathanail, A., Most, E. R., & Rezzolla, L. 2017, MNRAS, 469, L31
- Preparata, G., Ruffini, R., & Xue, S.-S. 1998, A&A, 338, L87
- Rezzolla, L., Giacomazzo, B., Baiotti, L., et al. 2011, ApJL, 732, L6
- Ruderman, M. A., & Sutherland, P. G. 1975, ApJ, 196, 51
- Rueda, J. A., Ruffini, R., Karlica, M., Moradi, R., & Wang, Y. 2019, arXiv e-prints, arXiv:1905.11339
- Rueda, J. A., Ruffini, R., Wang, Y., et al. 2018, JCAP, 10, 006
- Ruffini, R., Karlica, M., Sahakyan, N., et al. 2018a, ApJ, 869, 101
- Ruffini, R., Melon Fuksman, J. D., & Vereshchagin, G. V. 2019a, arXiv e-prints, arXiv:1904.03163
- Ruffini, R., Vereshchagin, G., & Xue, S.-S. 2010, PhR, 487, 1
- Ruffini, R., Vereshchagin, G. V., & Xue, S. S. 2016a, Ap&SS, 361, 82
- Ruffini, R., & Wheeler, J. A. 1971, Phys. Today, 24, 30
- Ruffini, R., & Wilson, J. R. 1975, PhRvD, 12, 2959
- Ruffini, R., Wang, Y., Enderli, M., et al. 2015, ApJ, 798, 10
- Ruffini, R., Rueda, J. A., Muccino, M., et al. 2016b, ApJ, 832, 136
- Ruffini, R., Rodriguez, J., Muccino, M., et al. 2018b, ApJ, 859, 30
- Ruffini, R., Moradi, R., Rueda, J. A., et al. 2018c, ArXiv:1803.05476
- Ruffini, R., Becerra, L., Bianco, C. L., et al. 2018d, ApJ, 869, 151
- Ruffini, R., Rueda, J. A., Moradi, R., et al. 2018e, arXiv e-prints, arXiv:1811.01839
- Ruffini, R., Li, L., Moradi, R., et al. 2019b, arXiv:1904.04162
- Sturrock, P. A. 1971, ApJ, 164, 529
- von Kienlin, A. 2013, GCN Circ., 14473
- Wald, R. M. 1974, Phys. Rev., D10, 1680
- Wang, Y., Rueda, J. A., Ruffini, R., et al. 2019, ApJ, 874, 39
- Wilson, J. R. 1978, in Physics and Astrophysics of Neutron Stars and Black Holes, ed. R. Giacconi & R. Ruffini, 644–675
- Xu, D., de Ugarte Postigo, A., Schulze, S., et al. 2013, GCN Circ., 14478